ResearchGate

See discussions, stats, and author profiles for this publication at: https://www.researchgate.net/publication/223468263

On the origin of El Chichón volcano and subduction of Tehuantepec Ridge: A geodynamical perspective

Article *in* Journal of Volcanology and Geothermal Research · August 2008

DOI: 10.1016/j.jvolgeores.2008.02.028

CITATIONS
34

READS
291

2 authors:

Marina Manea
Universidad Nacional Autónoma de México
69 PUBLICATIONS **744** CITATIONS
SEE PROFILE

vlad constantin Manea
Universidad Nacional Autónoma de México
84 PUBLICATIONS **1,250** CITATIONS
SEE PROFILE

Some of the authors of this publication are also working on these related projects:

National Laboratory for Advanced Scientific Visualization View project

Analysis of Geothermal Reservoirs View project

All content following this page was uploaded by Marina Manea on 08 September 2017.

The user has requested enhancement of the downloaded file.

Journal of Volcanology and Geothermal Research 175 (2008) 459–471

Contents lists available at ScienceDirect

Journal of Volcanology and Geothermal Research

journal homepage: www.elsevier.com/locate/jvolgeores

On the origin of El Chichón volcano and subduction of Tehuantepec Ridge: A geodynamical perspective

Marina Manea [a,*], Vlad C. Manea [a,b]

[a] Computational Geodynamics Laboratory, Centro de Geociencias, Universidad Nacional Autonoma de Mexico, Campus Juriquilla, Queretaro, Mexico
[b] Seismological Laboratory, Caltech California, Pasadena, 91125, USA

ARTICLE INFO

Article history:
Accepted 12 February 2008
Available online 6 May 2008

Keywords:
Mexican subduction zone
Tehuantepec Ridge
mantle wedge
serpentinization
El Chichón

ABSTRACT

The origin of El Chichón volcano is poorly understood, and we attempt in this study to demonstrate that the Tehuantepec Ridge (TR), a major tectonic discontinuity on the Cocos plate, plays a key role in determining the location of the volcano by enhancing the slab dehydration budget beneath it. Using marine magnetic anomalies we show that the upper mantle beneath TR undergoes strong serpentinization, carrying significant amounts of water into subduction. Another key aspect of the magnetic anomaly over southern Mexico is a long-wavelength (~150 km) high amplitude (~500 nT) magnetic anomaly located between the trench and the coast. Using a 2D joint magnetic-gravity forward model, constrained by the subduction *P–T* structure, slab geometry and seismicity, we find a highly magnetic and low-density source located at 40–80 km depth that we interpret as a partially serpentinized mantle wedge formed by fluids expelled from the subducting Cocos plate. Using phase diagrams for sediments, basalt and peridotite, and the thermal structure of the subduction zone beneath El Chichón we find that ~40% of sediments and basalt dehydrate at depths corresponding with the location of the serpentinized mantle wedge, whereas the serpentinized root beneath TR strongly dehydrates (~90%) at depths of 180-200 km comparable with the slab depths beneath El Chichón (200-220 km). We conclude that this strong deserpentinization pulse of mantle lithosphere beneath TR at great depths is responsible for the unusual location, singularity and, probably, the geochemically distinct signature (adakitic-like) of El Chichón volcano.

© 2008 Elsevier B.V. All rights reserved.

1. Introduction

El Chichón is a young (~0.2 Ma) active volcano located within a relatively young (~3 Ma) volcanic arc, at 300–330 km from the Middle America Trench (MAT) where the Cocos slab depth is 200–220 km (Syracuse and Abers, 2006). Located at the NW end of a typical continental calc-alkaline arc, the Modern Chiapanecan Volcanic Arc (MCVA) (Damon and Montesinos, 1978), El Chichón presents a magma signature (K-rich), which is different than the alkaline rocks form Los Tuxtlas Volcanic Field (Nelson et al., 1995) and the calc-alkaline rocks form TMVB (Macías et al., 2003; Mercado and Rose, 1992). This character was associated with melting of the Cocos slab by De Ignacio et al. (2003). Also, previous studies suggest that El Chichón K-alkaline magmas are derived from partial melting of the subducting Cocos plate (Luhr et al., 1984; Rye et al., 1984), which interacted with the mantle wedge (Taran et al., 1998) and the crust (Tepley et al., 2000; Espíndola et al., 2000). The triple junction proximity between the North America, Cocos, and Caribbean plates was proposed by Nixon (1982) as a cause for the alkaline volcanism of El Chichón. Manea and Manea (2006) hypothesized that the position and the distinct K-alkaline volcanism at El Chichón volcano are related to the arrival of the highly serpentinized Tehuantepec Ridge (TR) beneath MCVA. As Scambelluri et al. (2001) observed, normally, wedge serpentinite would be relatively low in alkalis, but the fluids released during dehydration may be moderately rich in alkalis because they preferentially enter the fluid phase.

The TR is a prominent bathymetric feature located on the Cocos Plate, whose onshore prolongation intercepts the El Chichón volcano (Fig. 1). The ridge separates the Cocos Plate in two parts with distinct tectonic regimes and age. According to Klitgord and Mammerickx (1982), Wilson (1996) and Manea et al.

* Corresponding author.
E-mail address: marina_manea@yahoo.com (M. Manea).

0377-0273/$ – see front matter © 2008 Elsevier B.V. All rights reserved.
doi:10.1016/j.jvolgeores.2008.02.028

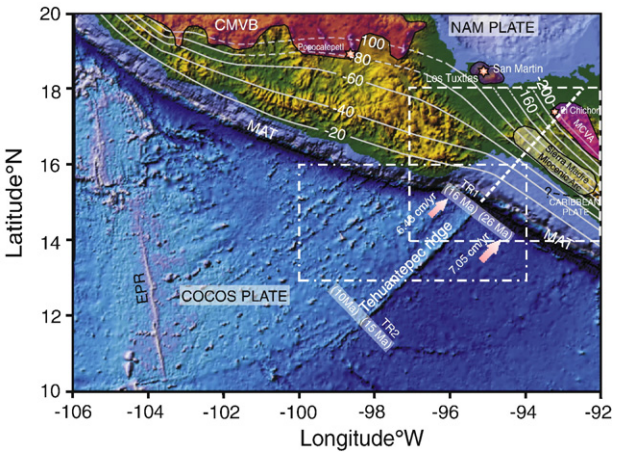

Fig. 1. Generalized tectonic map of the study area. Transparent red zones show the location of active volcanic belts in México: CMVB — Central Mexican Volcanic Belt, MCVA — Modern Chiapanecan Volcanic Arc. Transparent gray area: the extinct Sierra Madre Miocenic Arc. Orange stars are the El Chichón and San Martin active volcanoes. EPR — East Pacific Rise. MAT — Middle American Trench. Right black dashed line with a question mark is the hypothetical prolongation of Polochic–Montagua fault system which represents the limit between North America (NAM) and Caribbean plates. White dashed line is the onshore prolongation of Tehuantepec Ridge. Onshore white contours represent the slab isodepths (Bravo et al., 2004; Pardo and Suarez, 1995). Arrows show convergence velocities between the Cocos and North American plates (DeMets et al., 1994). TR1 and TR2 are the cross-sections where we calculate the thermal structure across TR (Fig. 10). Cocos plate ages are from Manea et al. (2005). White line dashed squares show the location of magnetic and gravity maps (Figs. 3, 5, 6). Blue dots represent continental heat-flow measurements (mW/m^2) from Ziagos et al. (1985).

(2003) the mean difference in age across TR varies from 7 to 12 Ma. It has been proposed that TR represents a major transpressional structure formed along a former transform fault on the Guadalupe plate 15–20 Ma ago and the northern boundary of a microplate embedded into the Cocos Plate (Manea et al., 2005). Another important characteristic that makes TR distinct from other fractures on the Cocos Plate is its linear shape, similar to the great fracture zones of the northeastern Pacific and Atlantic. In the Atlantic Ocean, transform faults intersect and offset the slow-spreading Mid-Atlantic Ridge system, and the hydrothermal circulation transforms the mantle peridotite into a 2–3 km thick serpentinite layer (Muller et al., 1997). Serpentinization of the oceanic mantle entering subduction zones around the Pacific has been proposed to occur along deep faults where oceanic plates bend upon entering into subduction (Peacock, 2001; Ranero et al., 2003) or along transform faults (Omori et al., 2002). Ranero et al. (2003) and Omori et al. (2002) suggest that partial serpentinization of the upper mantle offshore Nicaragua and Japan might exist up to depths of ~35 km and ~50 km, respectively. However, such extreme depths that extend to the entire oceanic lithosphere should be constrained by independent methods and measurements. Thermal structure of the oceanic lithosphere (controlled by age) may provide an important limitation on maximum depth extent of the serpentinized regions. The magnetic properties of serpentine are preserved only for temperature below Curie point (~580 °C) (Arkani-Hamed, 1989). The stability field for serpentine is also bounded by the ~600 °C isotherm (Hacker et. al, 2003), and therefore the serpentinization process might be identified and quantified by studying the magnetic anomalies. Magnetic measurements of ophiolites (Banerjee, 1980; Hall et al., 1987), spectral analysis of marine magnetic profiles (Harrison and Carle, 1981) and analysis of Magsat data over the Central American subduction zone (Vasicek et al., 1988), indicate that uppermost part of the oceanic upper mantle is magnetic. Fracture zones seem to be favorable places where mantle peridotite is altered to serpentinization, like Blanco Ridge in northeastern Pacific (Dziak et al., 2000). Placed in an active subduction system, these serpentinized ridges act like a temporary carrier of water: they store water through sea water infiltration and peridotite serpentinization. Then, as the subducting slabs dive into the asthenosphere and become hotter, the stored water is released back into the overlying mantle wedge. Here, the released fluids may partially serpentinize the mantle wedge peridotite, if the temperature is below 600 °C, which represents the upper limit of the serpentine stability field. At greater depths, where the mantle temperature approaches the wet-peridotite *solidus*, the fluids produced by the deserpentinization of oceanic lithosphere can induce partial melting. Also, oceanic sediments and oceanic crust represent another important fluid reservoir, and their metamorphic changes lead to fluid release into the mantle wedge, which enhance the serpentinization process. The serpentinization process not only produce magnetite and increase significantly the remanent magnetization (with an order of magnitude for 95% serpentinization (Saad, 1969)), but also greatly reduces the density by up to ~500 kg/m^3 (Christensen, 1966). Large parts of partially serpentinized mantle wedge can be seen in recorded gravity and magnetic anomalies over subduction zones. Indeed, a recent study of Blakely et al. (2005) shows the gravity and aeromagnetic signature of a serpentinized mantle wedge above Cascadia subduction zone, which extends down to ~60 km. Furthermore, they suggest that a serpentinized mantle wedge exists also in other subduction zones like Japan and Alaska. Another recent study of Manea and Manea (2006) proposes the presence of a "cold wedge" *P–T* structure beneath southern Mexico, as an explanation for the large distance between MCVA and the trench, and shows a good fit between the location of this "cold serpentinized wedge" and the low wavelength/high amplitude magnetic anomaly observed in this area.

With the help of available marine magnetic data, the present paper explores whether the uppermost part of the oceanic lithosphere beneath TR is serpentinized and try to quantify this phenomenon. Then we investigate, using constraints from magnetic data, gravity data and *P–T* structure of subduction zone, the existence of a serpentinized mantle wedge in southern Mexico. Finally, we integrate all the above results into a model, which provide a reasonable explanation on the origin and characteristics of El Chichón volcano, and its relationship with the TR subduction.

2. Tectonic and geological settings

Offshore, a main tectonic feature in southern Mexico is represented by TR, a major tectonic limit on the Cocos plate, along which the plate age sharply increases with 10 Ma at the MAT (Fig. 1). The rate of convergence between the Cocos plate and the North America plate in the vicinity of TR varies from 6.5 cm/yr to 7 cm/yr (DeMets et al.

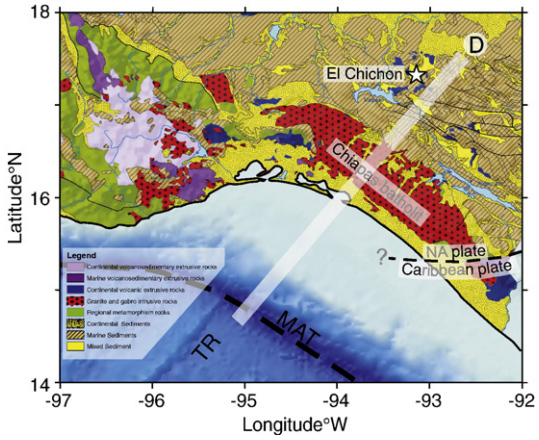

Fig. 2. Simplified geologic map of the study area. Transparent SW–NE profile (D) is the modeled cross-section. Other symbols are like in Fig. 1.

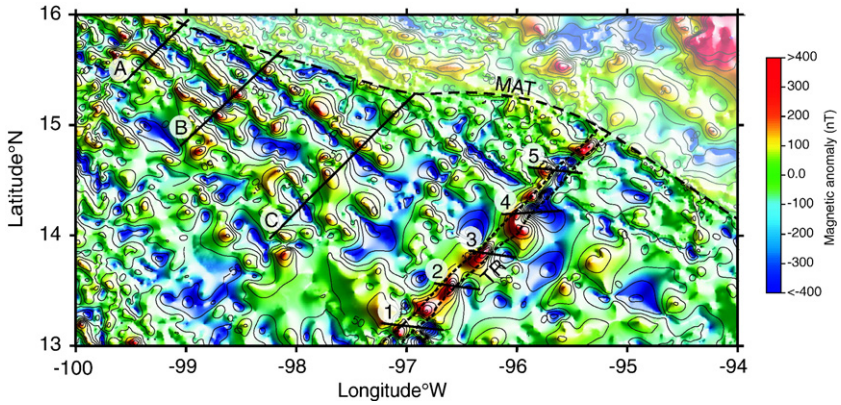

Fig. 3. Offshore magnetic map in the vicinity of TR. Dashed black line delineate the location of TR. Black straight lines represent the position of magnetic models shown in Fig. 8 and Fig. 9. Note the high amplitude magnetic anomalies located along TR.

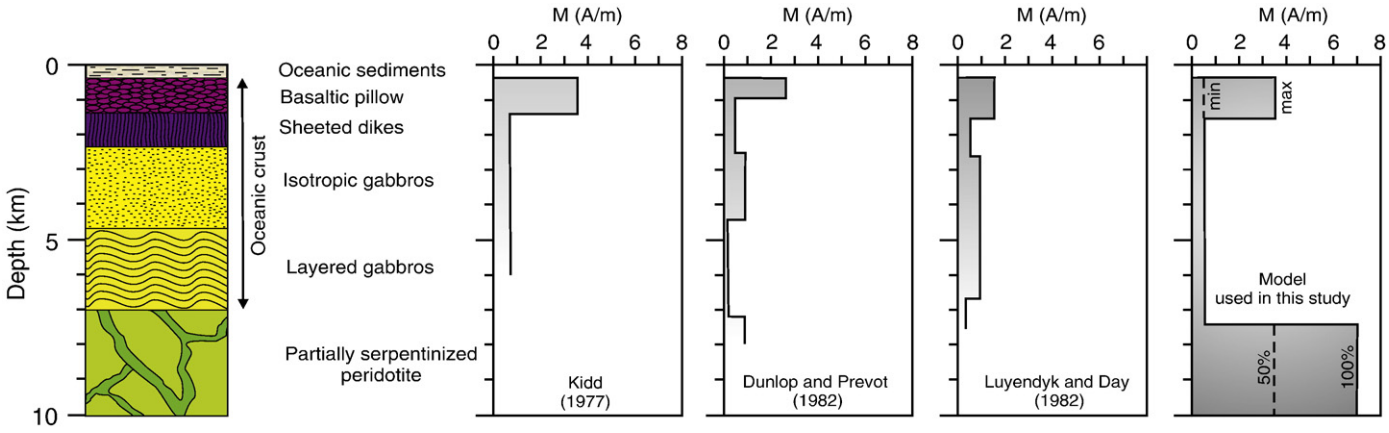

Fig. 4. Left: a typical oceanic plate structure. Right: ocean crust magnetization models proposed in literature and our simplified model used in this study.

(1994) — model NUVEL 1A). The geometry of Wadati–Benioff zone shows that the Cocos slab increases its dip from 25° NW of the TR, to ~40° southeast of TR (Rebollar et al., 1999; Bravo et al., 2004). Also the maximum depth extent of the intraslab earthquakes increases from 120 km to 240 km.

Previous studies erroneously reported a slab depth beneath El Chichón of 330 km (Garcia-Palomo et al., 2004). Also, the distance from the trench is incorrect in several studies related with El Chichón (400 km from the trench (Garcia-Palomo et al., 2004) and 390 km (Rebollar et al., 1999)). Using the Wadati-Beniof geometry of Bravo et al. (2004), who provide a better located seismicity beneath the Gulf of Tehuantepec, the slab depth beneath El Chichón is 200–220 km (using the correct distance from trench of 325 km). Onshore, the regional tectonics is dominated by the Chiapas Anticlinorium (where El Chichón is located), the Chiapas Massif, and the North America–Caribbean plate boundary marked by the Motagua–Polochic Fault System (Fig. 2). In this region, there are two volcanic arcs: the extinct Miocene Sierra Madre arc, which runs parallel to the coast, and the active MCVA farther inland. Damon and Montesinos (1978) showed that the Miocene Sierra Madre arc was abandoned between 9 and 3 Ma, then the MCVA was born as a consequence of a reorganization of the Cocos plate. The youngest member of MCVA is El Chichón volcano (~0.2 Ma), well known for its last violent eruptions of March–April 1982 which killed ~2000 people (Espíndola et al., 2000). To the NW and SE El Chichón is bordered by two large (250 km) volcanic gaps. There are several characteristics of El Chichón volcano, which makes it both mineralogically and geochemically distinct from the rest of the volcanoes in Mexico and Central America. While the Trans-Mexican Volcanic Belt to the northwest and the Central American Volcanic Arc to the southeast are composed primarily of calc-alkaline volcanic rocks, El Chichón has produced K-alkaline magmas (Garcia-Palomo et al., 2004).

3. Geophysical observations: gravity and magnetic anomalies

A recent 1×1 km^2 data grid of residual magnetic anomalies (relative to International Geomagnetic Reference Field (IGRF)) for this

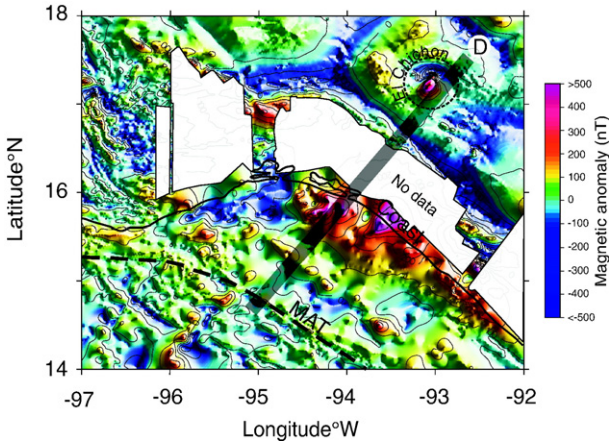

Fig. 5. Magnetic map over the study area and the modeled cross-section D. Note the high amplitude (~500 nT), long-wavelength (~150 km) magnetic anomaly along the coast (offshore). The map is not reduce to pole, that is the magnetic sources are not located just beneath the maximum. White regions represent areas with no data available.

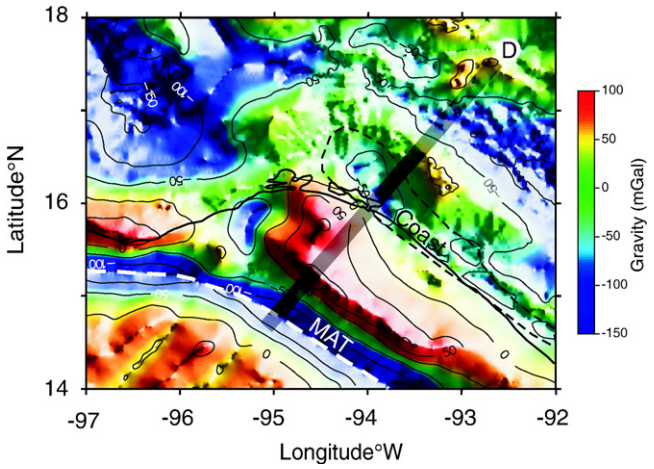

Fig. 6. Free air offshore and Bouguer onshore gravity map of the study area. The gravity low along the coast (onshore) marked by the dashed black contour. Other symbols are like in Fig. 5.

region is available from North American Magnetic Anomaly Group (2002). Onshore, the surveys were flown with dense line spacing ranging from 2 to 6 km and flight heights from 450 to 3350 m above sea level. The grid was converted from a constant (barometric) altitude to a constant elevation above terrain. The marine data were obtained from the National Geophysical Data Center of the National Oceanic and Atmospheric Administration and span the years 1958 through 1997. Gridding was performed to a final cell size of 1 km using a minimum curvature algorithm and a grid radius of 24 km to fill in the small no-data areas.

Offshore magnetic data over southern Mexico show a distinctive pattern, with high-amplitude magnetic anomalies over TR (Fig. 3) and the Pacific coast (Fig. 5). The magnetic anomalies over TR show high amplitudes of 200–300 nT and wavelengths of 20–30 km, whereas the rest of marine magnetic anomalies have shorter wavelengths (8–10 km) and lower amplitudes 100–200 nT. Also, the high amplitude magnetic anomalies are aligned just over TR, while the rest of magnetic lineations are sub parallel with MAT, and are related with geomagnetic reversals recorded in the oceanic crust. These former magnetic lineations are the product of oceanic crust generation at EPR, where as they cool below the Curie temperature the magnetic minerals in the crust record the ambient geomagnetic field (Vine and Matthews, 1963). Although the major contributor (50–75%) to these marine magnetic anomalies is the extrusive basaltic layer (Johnson and Atwater, 1977; Blakely, 1983; Tivey et al., 1998), natural remanent magnetization (NRM) of gabbros also contribute significantly to the recorded magnetic anomalies over oceans (Kent, 1975; Kent et al., 1978; Pariso and Johnson, 1993). There are several models of magnetic layer thickness: an upper magnetic layer thickness varying from 0.5 to 1 km and magnetization from 1.5 A/m to 3.5 A/m, followed by an intermediate 5–6 km layer with 0.5–1 A/m (Fig. 4) (Kidd, 1977; Dunlop and Prevot, 1982; Luyendyk and Day, 1982). Also Blakely et al. (2005) used for the gravity-magnetic models of the Oregon forearc an oceanic crust with magnetic intensities of 0.55–2.20 A/m. We use in this study a simplified magnetic model for the oceanic crust composed by three layers, a 1 km thick upper layer with a magnetization of 0.5–3.5 A/m, followed by a 6 km thick and less magnetic layer (0.5 A/m), and a partially serpentinized layer with variable thickness. These values of magnetization are consistent with sample measurements of Hayling and Harrison (1986), who measured a NRM for basalts of 5.37 A/m and 0.478–0.631 A/m for unaltered gabbro. We include in our model (Fig. 4) a layer with variable thickness of partially serpentinized peridotite just beneath the oceanic crust with a NRM of up to 7 A/m which represents fully serpentinized mantle. This high value of magnetization is consistent with rock measurements of Fox and Opdyke (1973) (NRM=7.86 A/m) and Hayling and Harrison (1986) (NRM=6.03 A/m).

Onshore, the highly magnetic forearc region (Fig. 5) is not in phase with the high-gravity region (Fig. 6), even though it is known that, usually, magnetic rocks have high densities (Blakely et al., 2005). Actually, the high-magnetic region is displaced well east of the high-gravity area. This situation is similar with the Cascadia subduction zone where a similar pattern was observed by Blakely et al. (2005), although in southern Mexico the magnetic amplitude is higher (~500 nT compared with only ~200 nT). Also, the Mexican high-magnetic anomaly has a larger wavelength of ~150 km. Blakely et al. (2005) show that the unusual configuration and shape of gravity and magnetic anomaly in Cascadia can be explained by the presence of a serpentinized mantle wedge located between the slab surface (35–60 km depth) and the Moho (~35 km depth). The main problem with the onshore magnetic anomalies in southern Mexico is the lack of data in some areas (Fig. 5). However, most of the long wavelength magnetic anomaly is recorded and only the shallow magnetic sources beneath the data gaps cannot be constrained.

4. Geophysical models

4.1. Magnetic thickness model over TR

Although the offshore magnetic map shows a chain of high amplitude anomalies located over TR (Fig. 6), part of the recorded magnetic signal might contain a significant contribution from the

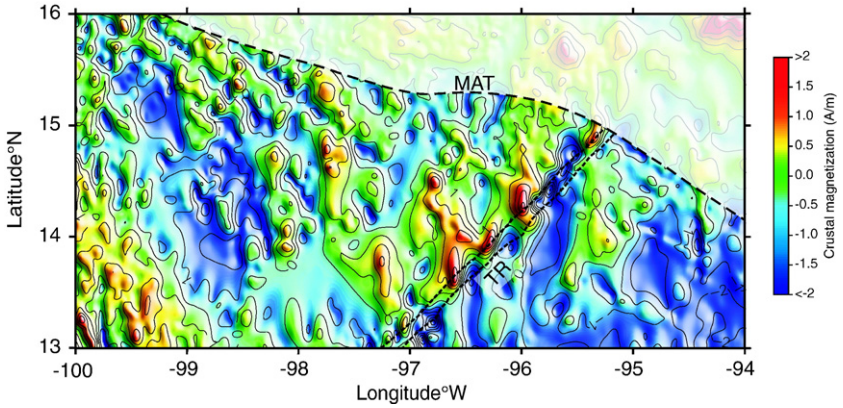

Fig. 7. Average crustal magnetization stored in the oceanic crust (7 km thick) obtained using the Parker inversion technique applied to the magnetic anomaly shown in Fig. 3. Distinguish the highly magnetized areas distributed along TR, indicating a magnetic source beneath the ridge.

bathymetric expression of the TR. In the presence of strong bathymetric discontinuities it is useful to perform an inversion of magnetic anomalies to infer the average amount of magnetization stored in the oceanic crust. A good approach is to use the Parker inversion, a commonly used method to infer crustal magnetization in the presence of topography (Parker and Huestis, 1974). This method assumes a magnetized layer constant thickness of which the lower surface follows the oceanic bathymetry. Within this magnetic layer the direction of magnetization is assumed to be constant, and the magnetic intensity is allowed to vary only in the horizontal direction. We used a 7 km thick layer and the magnetization direction of a field caused by the present-day axial dipole. The result of the inversion is presented in Fig. 7, and shows a series of highly magnetized regions (>2 A/m) aligned along TR. Actually the TR magnetization is almost double than the magnetization of magnetic lineations to the north. This result indicates that the high magnetic anomalies over TR are not caused by the bathymetry but rather they come from deep-seated rocks beneath the ridge or compositional changes of the rocks forming the ridge.

We performed a forward magnetic model for a series of 8 magnetic profiles, 3 of them located north of TR and normal to the magnetic lineations, and 5 of them across TR (Fig. 3). The results show a reasonably good fit with the observed anomalies, suggesting that a shallow thin basaltic layer and a deeper and thicker gabbro layer are the major contributors to magnetic anomalies in the oceanic crust (Fig. 8). On the other hand, the anomalies over TR cannot be fit solely by the basaltic and gabbro layers, and an additional serpentinized root should be added beneath TR (Fig. 9). The results show a better fit between the observed and modeled magnetic anomaly if a high magnetization (~7 A/m) is used for the serpentinized root beneath TR. In a previous study, Manea et al. (2003) introduced a low-density root (2800 kg/m^3) beneath TR in order to adjust the gravity anomaly along a profile normal to the ridge. This is consistent with our results, since the serpentinized peridotite not only has high magnetization but also a low density of ~2800 kg/m^3. We used a serpentinized root with a thickness of 5–6 km, consistent with the low-density root thickness from Manea et al. (2003). The maximum depth of serpentinized root does not exceed the calculated Curie isotherm (600 °C) beneath TR (22–26 km) (Fig. 10). We conclude at this point that a highly serpentinized root might exist beneath TR, and therefore significant amounts of H_2O could be transported into the subduction system.

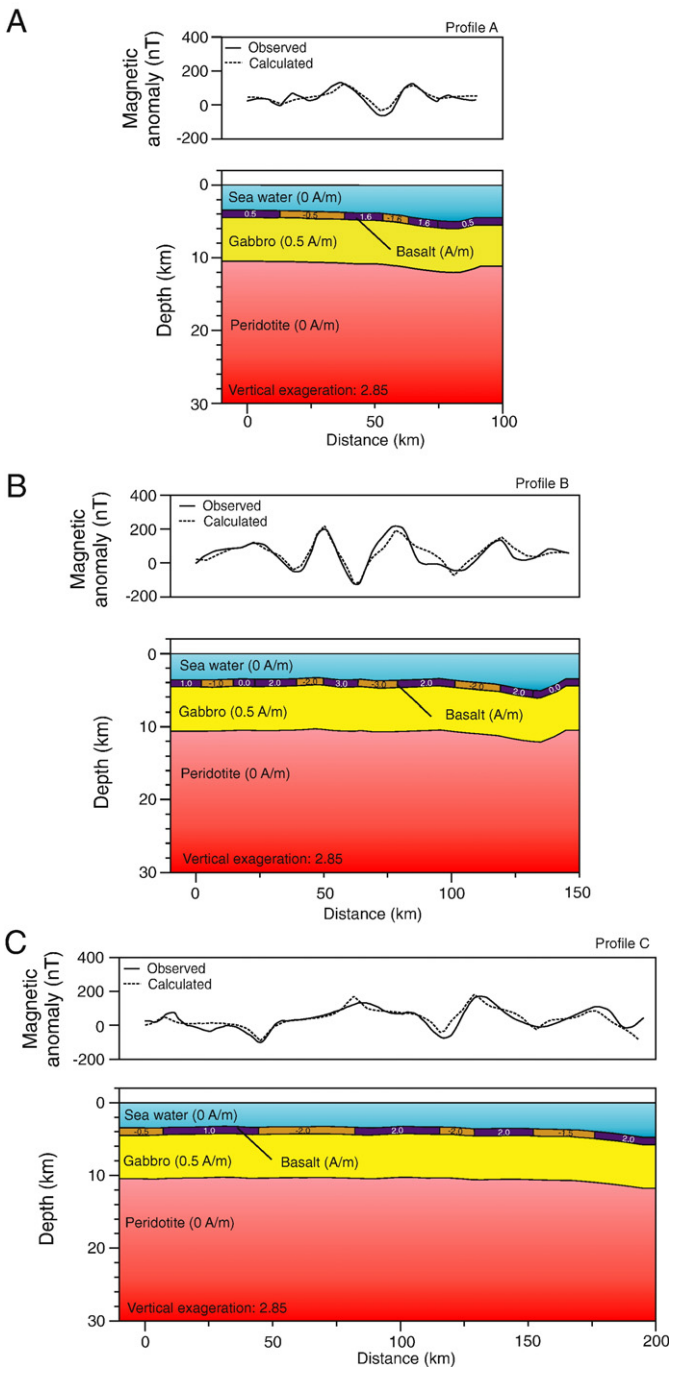

Fig. 8. Modeling results for three magnetic profiles (A, B,C — see Fig. 3) normal to the magnetic lineations on the Cocos plate. A shallow thin basaltic layer and the thicker gabbro layer are the major contributors to magnetic anomalies in oceanic crust north of TR.

4.2. 2D thermal models and mantle wedge serpentinization

In this study we developed a series of thermal models for the subduction zone along the onshore prolongation of the TR (Profile D in Fig. 5). The model is constrained by seismic data (Rebollar et al., 1999; Engdahl and Villaseñor, 2002), convergence rate (DeMets et al., 1994) and oceanic plate age at the MAT (Klitgord and Mammerickx, 1982; Kanjorsky, 2003; Manea et al., 2005) (Fig. 1). The modeling procedure is described in detail in Manea et al. (2005). We use a strong temperature dependence of upper mantle viscosity in all the models. Also, we allow the mantle flow not to penetrate the whole wedge tip, by imposing a certain limit which allow us to create cold mantle wedges with different sizes. The benchmark results are presented in APENDIX A. The portion of the mantle wedge delimited by Moho, slab surface and the 600 °C isotherm (Curie isotherm) is used to forward modeling the magnetic and gravity response of a serpentinized wedge alone, and compare it with the observed anomalies. Our best estimate is presented in Fig. 11, where a serpentinized mantle wedge extending to ~80 km depth has a magnetization of 5 A/m and a density of 3000 kg/m^3. If we assume that a high magnetization of 7 A/m and a low density of 2700 kg/m^3 (3300 kg/m^3 corresponds for 0% serpentinization) correspond to a fully serpentinized wedge, then our estimates suggest that the mantle wedge is ~50–70% serpentinized.

4.3. 2D magnetic and gravity forward model

It is known that deep magnetic sources produce anomalies at the surface with long wavelengths. Before proceeding with the simultaneous gravity and magnetic forward modeling we infer the

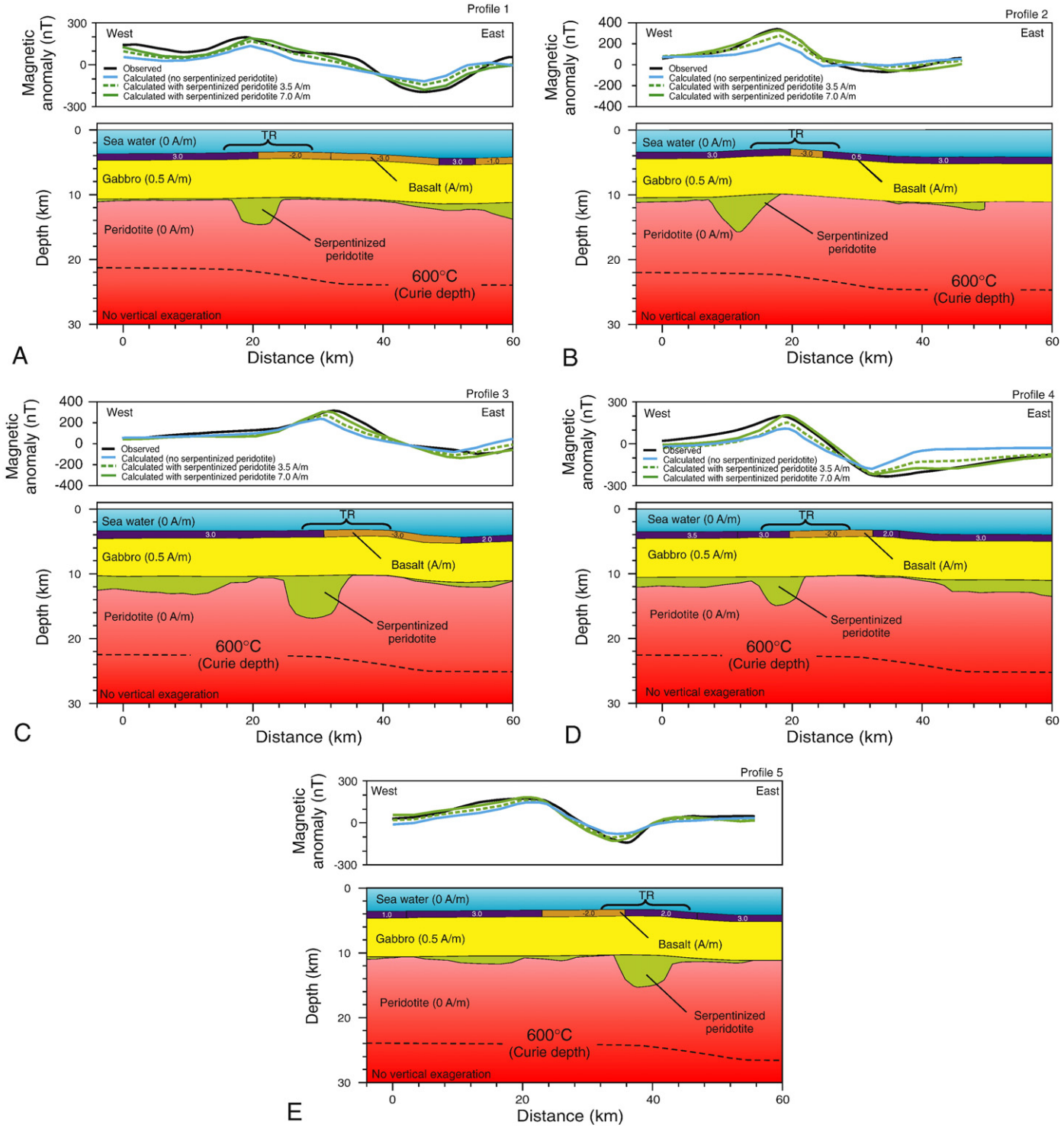

Fig. 9. Modeling results for five magnetic profiles (1, 2, 3, 4, 5 — see Fig. 3) across TR. An additional ~5 km thick highly magnetic serpentinized root need to be added beneath TR in order to fit the observed magnetic anomaly.

approximate location (center of mass) of the magnetized body responsible for the unusual large magnetic anomaly. We use the spectral method (Blakely, 1995), which is able to separate the deep and shallow sources as function of wavelength, λ (or wavenumber $k=2\pi/\lambda$) and the energy carried in each wavelength. The results of spectral analysis is presented in Fig. 12. Two major trends can be identified, one for long wavelengths (λ>50 km), which corresponds to deep sources, and another one for short wavelengths (λ<10 km), which accounts for shallow magnetic sources. The slope of each trend provides a coarse estimate of the depth of magnetized bodies. Contribution from a deep source located at ~50 km is responsible for the long wavelength component seen in the magnetic anomaly, whereas shallow sources at ~10 km produce the shorter wavelengths. The deep source center of mass located at ~50 km depth is consistent with our estimate of a serpentinized wedge delimited by the

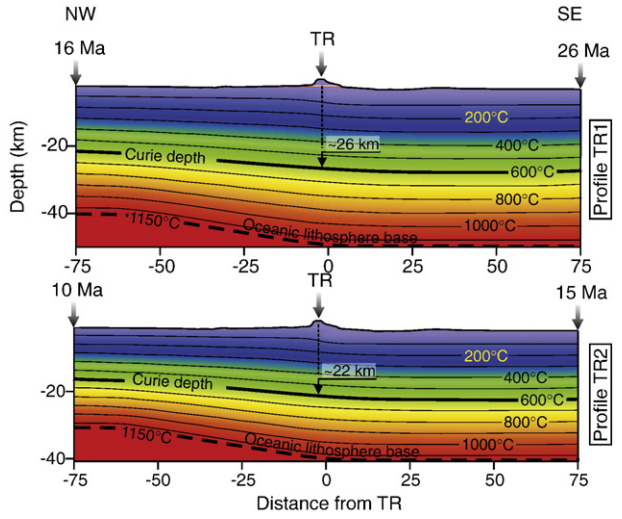

Fig. 10. Thermal structure across TR for two profiles, TR1 and TR2, shown in Fig. 1. The heat transfer is considered to be only by conduction. The Curie depth (equivalent to 600 °C isotherm) beneath TR varies from 22 km to 26 km.

Moho, the slab surface, the 600 °C isotherm and extending down to ~80 km (Figs. 11 and 13).

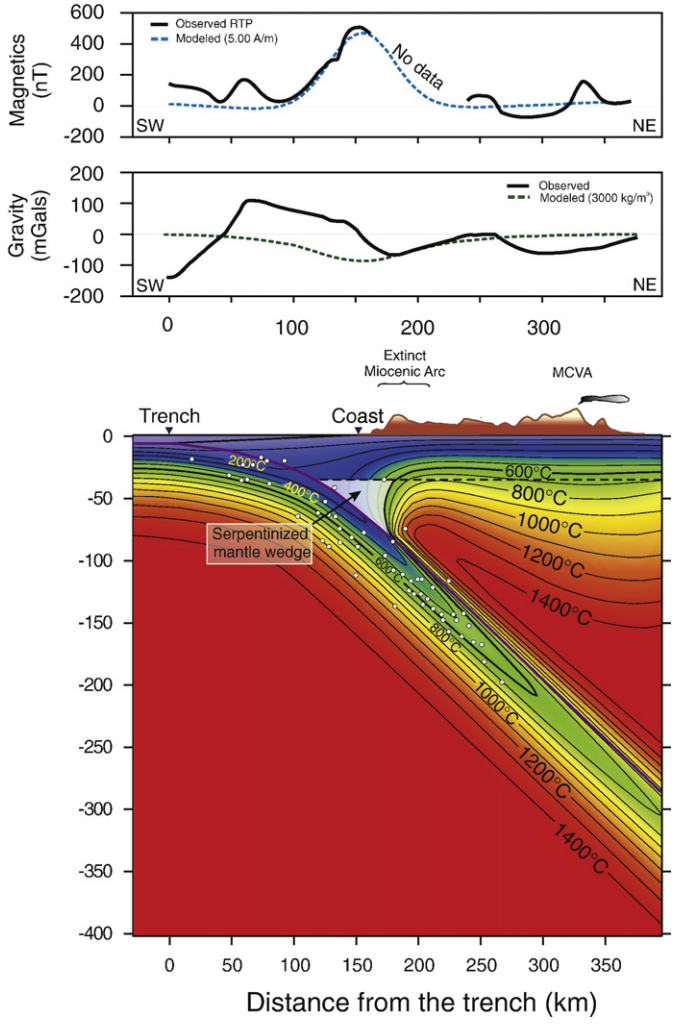

Fig. 11. Best fitting thermal model across the profile D shown in Fig. 5 (from Appendix A). The semitransparent triangle represents the proposed serpentinized mantle wedge. White dots are the intraslab earthquakes used to constrain the slab geometry (Rebollar et al., 1999).

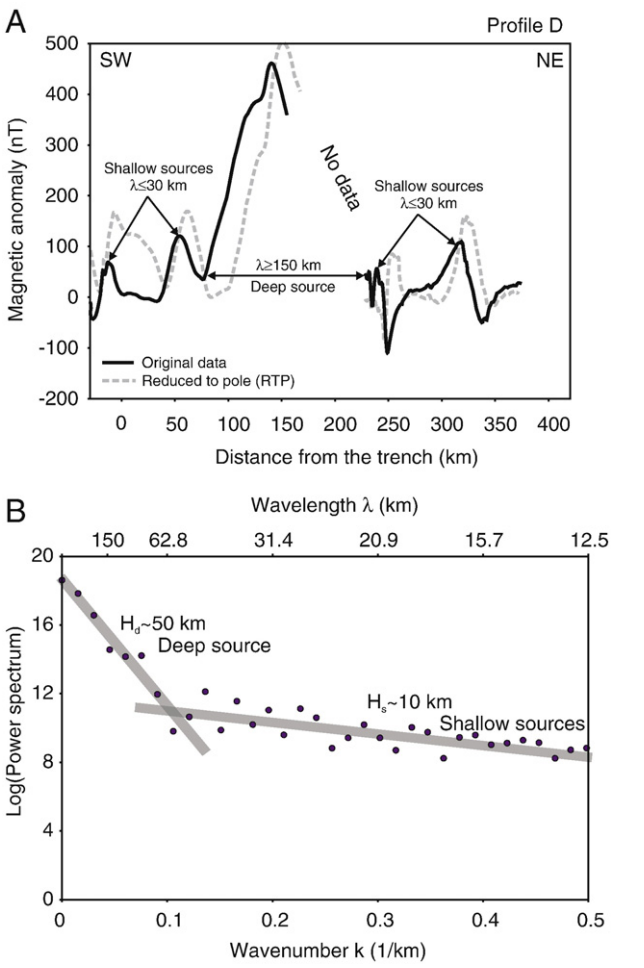

Fig. 12. The results of spectral analysis applied for the magnetic anomaly across the profile D shown in Fig. 5. A — original (black continuous line) and reduced to pole (dashed gray line) magnetic anomaly. Where no data are available we performed a spline interpolation. B — we identified a deep magnetic source located at ~50 km and a shallow magnetic sources at ~10 km.

We developed a joint gravity and magnetic forward model of the southern Mexico forearc along a profile shown in Fig. 5, which includes not only the serpentinized mantle wedge. The parameters (density and magnetization) used in the modeling are presented in Table 1, according with the model of Blakely et al. (2005). The continental Moho is placed at ~28.5±3.5 km in agreement with seismic studies in the region (Bravo et al., 2004) and the shape of the slab is constrained by seismicity (Bravo et al., 2004). Also, the updip limit of the serpentinized mantle wedge is constrained by rupture areas of past subduction earthquakes. Key aspects of the best fitting 2D thermal model were introduced (Fig. 11): the position of the 600 °C Curie isotherm, an initial geometry of the serpentinized mantle wedge and its magnetic and density properties (5 A/m and 3000 kg/m^3). We use the geologic map of Mexico (Fig. 2) to introduce in our modeling relevant features like the Chiapas batholith and a thick sedimentary layer. A reduced to pole (RTP) magnetic anomaly was employed, because the source and the magnetic maximum are vertically aligned and therefore removing one level of complexity from the interpretation process. We fit the short magnetic wavelengths by introducing highly magnetized bodies (1 A/m) in the upper part of the crust (<15 km). Using a quantitative model of southern Mexican convergent margin, based on both gravity and

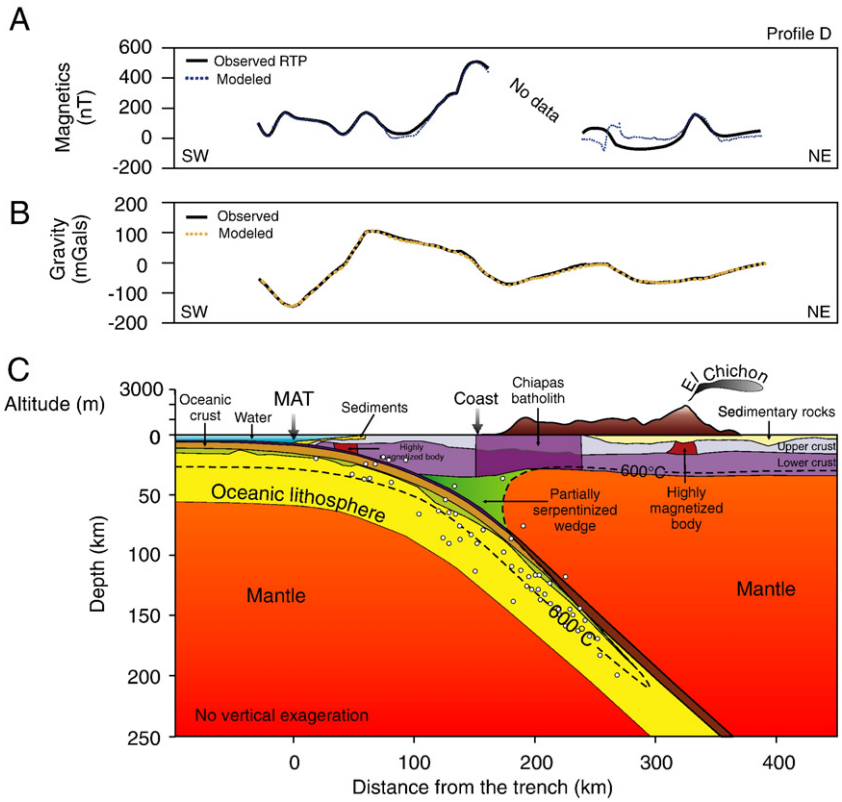

Fig. 13. Simultaneous gravity and magnetic model across profile D. A: Magnetic profile extracted from Fig. 5. B: Gravity profile extracted from Fig. 6. C: Crust and upper-mantle model. White dots are the intraslab earthquakes used to constrain the slab geometry (Bravo et al., 2004). See Table 1 for physical properties used in the model.

magnetic anomalies, we find that a serpentinized mantle wedge (50–70% serpentinization) reasonably explains the particularities of potential-field anomalies in the study area.

5. Subduction of TR and mantle hydration

An important key process related with arc magmatism is the subduction zone water cycle, the hydration–dehydration of oceanic lithosphere. The water carrier into the subduction zone is the oceanic plate (sediments, oceanic crust and serpentinized peridotite). There are several key places where the hydration process actually takes place: it is maximum at the mid-ocean ridges (i.e. EPR) and then gradually decreases as the ocean plate becomes older. Other places where hydration might occur are the fracture zones, transform faults and along deep faults where the oceanic plates bend before being subducted (Peacock, 2001; Omori et al., 2002; Kerrick, 2002).

We have shown in the previous chapters that the mantle peridotite beneath TR can be highly serpentinized, and therefore significant water quantities are transported deep into the subduction system, if the slab temperature is below the choke point, 600 °C at 6 GPa (Kawamoto et al., 1996). Also, basalt and sediments-water systems play an important role in transporting and discharging water into the mantle. Based on the preferred thermal model (Fig. 11) and phase diagrams from Rüpke et al. (2004) we analyze the stability of hydrous phases and estimate the water content in the descending Cocos slab in the vicinity of TR. We also analyze the depth intervals where various hydrous phases break down, and compare them with the slab depth beneath El Chichón volcano (200–220 km) and underneath the proposed serpentinized mantle wedge (40–80 km).

Table 1
Physical rock properties used in the combined 2D gravity-magnetic forward model (Fig. 14)

Unit	Density (kg/m^3)	Magnetization (A/m)
Water	1030	0.0
Oceanic sediments	2200	0.0
Continental sediments	2400	0.1
Continental upper crust	2670	0.5
Continental lower crust above Curie isotherm	3090	0.1
Continental lower crust below Curie isotherm	3090	0.0
Chiapas batholit	2670/3090	0.8
Oceanic crust — basalt	2900	5.0
Oceanic crust — gabbro	2900	0.5
Oceanic lithosphere	3340	0.0
Serpentinized oceanic lithosphere	2800	7.0
Serpentinized mantle wedge	3000	5.0
Mantle	3300	0.0
Highly magnetized body 1	2670	0.8
Highly magnetized body 2	3090	0.8

5.1. Sediment–water system

Although the young Cocos plate holds a relatively thin sediment layer (200–400 m), oceanic sediments can be one of the major water transporters into the upper mantle (Ono, 1998). Fig. 14A presents the estimation of H_2O amount retained by minerals in sediments as function of *P–T*. Sediments start to dehydrate at ~60–70 km, and by ~80 km, which is the downdip limit of the modeled serpentinized mantle wedge, they have already lose ~50% of their water content. The stable hydrous phase in sediments at higher depths (200–250 km) is phengite, which at 8 GPa transforms into topaz–OH, decreasing the H_2O content from 2 wt.% to 0.7 wt.%. A total of ~2 wt.% H_2O is released

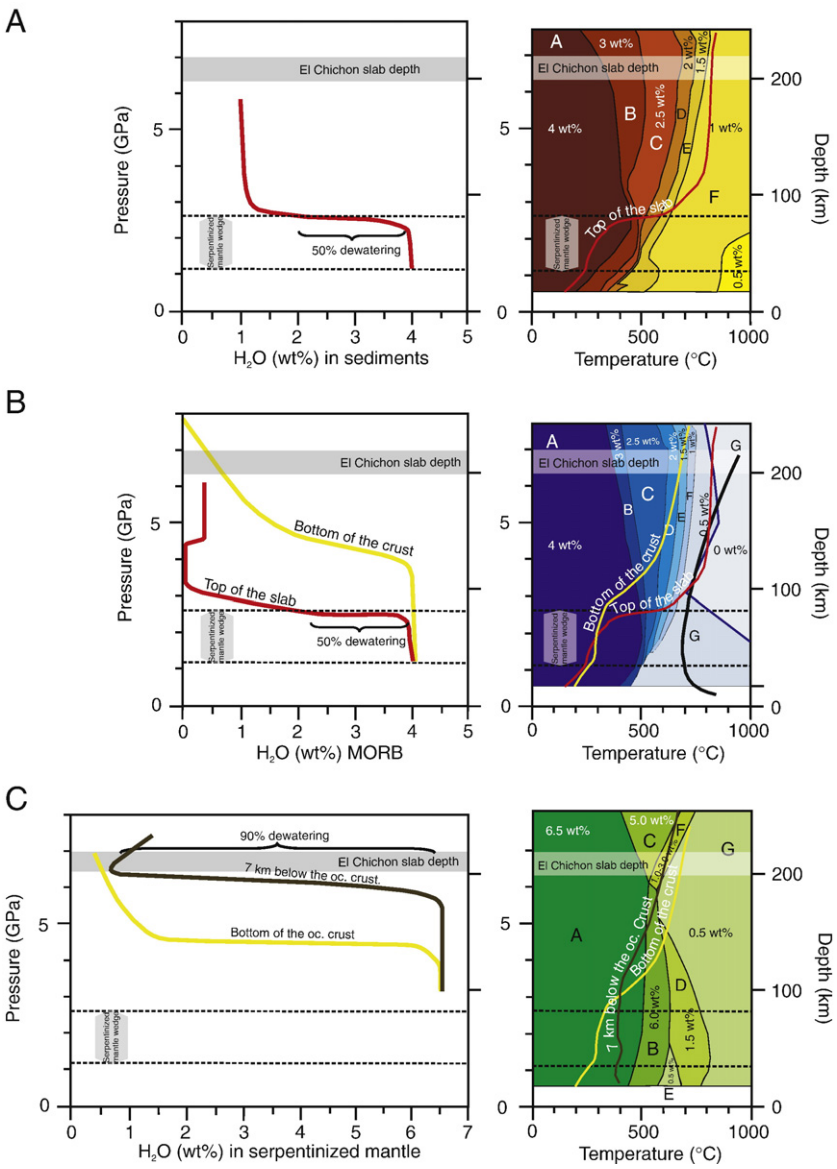

Fig. 14. Computed phase equilibria and *P–T* water content plots for the three different slab fluid sources: sediments, metabasalt, and serpentinized mantle (Rüpke et al., 2004). Top of the slab, bottom of the oceanic crust and 7 km below the oceanic crust geotherms (from computed *P–T* structure in Fig. 11) are shown. Also the slab depths (200–220 km) beneath El Chichón and the serpentinized wedge slab depths (40–80 km) are indicated in each plot.

into the overlying mantle at depths where we propose the existence of the serpentinized wedge. Although the sediment–water systems seem to be able to transport water to greater depths (~1 wt.% H_2O at 200 km), the small amount of subducted sediments in southern Mexico suggest that they cannot account for partial melting of the mantle peridotite beneath MCVA and El Chichón.

5.2. Basalt–water system

We use the phase diagram for metabasalt of Rüpke et al. (2004) and top and bottom oceanic crust (7 km thick) isotherms from the thermal model presented in Fig. 11. From Fig. 14B we can see that the upper part of oceanic crust dehydrates ~50% into the mantle wedge and the amount of water released by the oceanic crust between 70 km and 80 km is ~2 wt.%. Then, at higher depths, the oceanic crust dewaters gradually and continuously down to ~240 km, and another ~2 wt.% is delivered into the overlying mantle. At these depths the stable hydrous phase is lawsonite, which disappears at 9 GPa and 700 °C. There is no significant amount of water released at depths where El Chichón projects onto the slab surface (200–220 km), as most dehydration occur at 100–150 km depth. Also the top of the slab intersects the wet *solidus* for basalt at 100–150 km depth.

5.3. Peridotite–water system

The peridotite layer of subducting slabs contains water due to serpentinization along fracture zones (Ohtani, 2005). The degree of serpentinization is not well known, Schmidt and Poli (1998) estimate that the upper 5 km of the peridotite layer is only 10% serpentinized, whereas other studies suggest more intensive serpentinization (Kesson and Ringwood, 1989). Although serpentine might be the principal hydrous phase in upper mantle peridotite, chlorite and phase 10 Å are also

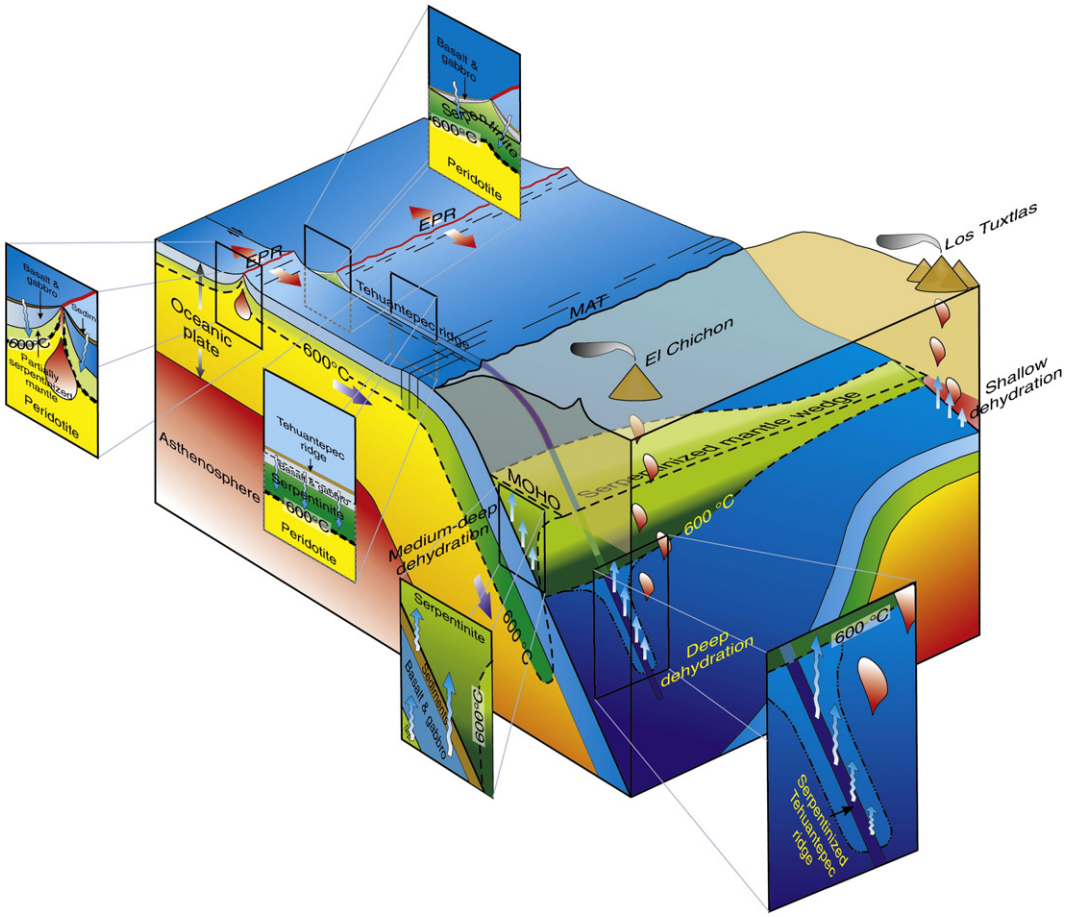

Fig. 15. Tectonic model for southern Mexican subduction zone showing where serpentinization–deserpentinization processes might occur. Large red and blue arrows indicate relative plate motion. Vertical light blue arrows depict fluid access or discharge. Red drops represent magma. Black lines along EPR, TR and MAT show the presumably location of fractures which cut deep into the oceanic lithosphere. The serpentinized oceanic lithosphere beneath TR carries water into subduction zone and releases it at greater depths of 180–200 km (deep dehydration). Sediments and oceanic crust participate with fluids to serpentinize the mantle wedge (medium-deep dehydration).

important candidates for water carriers into subduction zones. The amount of water stored into all these three hydrous phases is estimated by Schmidt and Poli (1998) at 4.1–6.5 wt.%, and is stable up to 8 GPa (~240 km). To estimate the H_2O amount stored into the serpentinized subducting lithosphere beneath El Chichón, we combine two slab geotherms, located at the base of oceanic crust and 7 km below, with the phase diagram for serpentinized mantle (Rüpke et al., 2004). The results presented in Fig. 14C show that a significant amount of water (6.5 wt.%) is preserved in the serpentinized peridotite layer down to 160–180 km depth. There is no water release from the serpentinized peridotite layer beneath TR at depths corresponding to the serpentinized mantle wedge (40–80 km). At higher depths, the slab crosses the choke point, 600 °C at 6 GPa (Kawamoto et al., 1996) or 700 °C at 7 GPa (Poli and Schmidt, 2002), a strong dehydration process occurs and ~90% of the fluid is released. This is a significant result since the slab depth beneath El Chichón is 200–220 km, and therefore it suggests that the strong serpentine dehydration beneath the subducted TR can cause partial melting of the mantle above the slab. The difference between the slab depth beneath El Chichón and the depth where the serpentinized oceanic lithosphere releases fluids (~20 km), can be explained by the time necessary for the released water to cross the oceanic crust and to run off the slab into the overlying mantle at 200–220 km depth.

6. Discussion and conclusions

In this study we try to shed some light on the origin of El Chichón volcano, and our approach is to link its singularity with TR, also a major discontinuity on the Cocos plate. The “toolbox” used here contains the following items: magnetic and gravity data, geologic and tectonic maps of the study area, subduction *P–T* structure beneath El Chichón, phase diagrams for sediment-, basalt-, and peridotite-water systems, and several techniques like Parker inversion, 2D combined magnetic-gravity forward modeling and thermal modeling of subduction zones.

The magnetic map (Figs. 3, 5) over southern Mexico reveals several key features: a series of high amplitude magnetic anomalies (300–400 nT) aligned just above TR, almost double than the rest of magnetic lineations in the nearby area, and a prominent long-wavelength (~150 km) high-amplitude (~500 nT) anomaly situated over the southern Mexican coast.

Using a Parker inversion approach (Parker, 1973), we show that the strong magnetic anomaly signal over TR has a highly magnetized source which is not due to bathymetry effects (Fig. 7). Using a standard magnetization model for the oceanic crust (Fig. 4) and a forward modeling approach to fit the observed magnetic data, we propose the existence of a highly serpentinized root beneath the TR. Because serpentine not only is highly magnetic but also low-density (~2800 km/m3), our result is consistent with

the previous study of Manea et al. (2003), where a low-density root is introduced beneath TR to fit the observed gravity anomaly. Serpentinite is common where transform faults intersect and offset slow-spreading systems like Mid-Atlantic Ridge (Kerrick, 2002), and is not frequent in the fast-spreading ridges of the Pacific oceanic plate (O'Hanley, 1996). Indeed, TR is located on the prolongation of Clipperton fracture zone which offsets the EPR with ~100 km, but EPR is a very fast spreading system, apparently contradicting and challenging our results. Manea et al. (2005) studied the tectonic evolution of TR, and proposed an episode of deceleration (~2 cm/yr) between 10–15 Ma of the Cocos plate just south of Clipperton fracture zone. Also, they propose the existence of a period of intense transpressional deformation which actually reshaped the fracture zone into TR. The combination of these two events, coupled with a large offset of the spreading center 10–15 Ma ago, could provide the necessary background for upper mantle serpentinization. The shape of the serpentinized mantle beneath TR is not well constrained in our models, because of the nature of potential fields which cannot produce unique results. However, we estimate a serpentinized root of ~5 km thick wide located beneath TR, into the upper part of the oceanic lithosphere (Fig. 9). The degree of serpentinization is also uncertain, but the large intensity of magnetization (7 A/m) used in our models, and a low density (2800 kg/m^3) used in a previous study, suggest a highly serpentinized root.

Another important observation depicted in the magnetic map, is the presence of a high amplitude and long wavelength magnetic anomaly located between MAT and the coast (Fig. 5). We performed a preliminary analysis in order to obtain an approximate location of the source. Using a spectral analysis technique, we propose the existence of a deep magnetic source, of whose center of mass is located at ~50 km depth (Fig. 12). Then, a benchmark of combined 2D gravity-magnetic forward model and 2D thermal modeling are used to preliminary constrain the shape and depth of this magnetic source (Appendix A). The best-fitting model (Fig. 11) reveals the existence of a highly magnetic low-density body delimited by the slab surface, Moho and the location of the Curie isotherm 600 °C. Such peculiar properties are specific for serpentinized rocks, and therefore we propose that a significant portion of the mantle wedge beneath southern México is partially serpentinized (50–70%). These results are consistent with the interpretation of seismic results of Bostock et al. (2002) for the Cascades subduction zone, where they estimate the mantle wedge to be 50–60% serpentinized.

To find the sources of serpentinization, we study the dehydration evolution along the subducting slab beneath El Chichón. Using phase diagrams for sediment-, basalt- and peridotite-water systems (Rüpke et al., 2004) together with the subduction *P–T* structure (Fig. 11), we conclude the following:

1) Sediments dehydrate first, dewatering ~50% into the mantle wedge at depths corresponding to the location of serpentinized mantle (40–80 km) (Fig. 14A).
2) Upper parts of the basaltic oceanic crust dehydrates ~50% into the serpentinized wedge and into the mantle at depth of 100–150 km (Fig. 14B). Also, the upper part of the oceanic crust intersects wet-*solidus* at 100–150 km.
3) Serpentinized oceanic lithosphere dehydrates at great depths of 180–200 km, where ~90% of the stored water is released when the slab crosses the choke point (600–700 °C at 6–7 GPa) (Fig. 14C). This correspond to the slab depth beneath El Chichón (200–220 km).

In Fig. 15 we show a plate model where a synthesis of slab hydration and dehydration spots in the southern Mexican subduction system is presented. One of the first places where the Cocos plate might be exposed to serpentinization is the transform fault related with the Clipperton fracture zone. Also, the parallel fracture system in the vicinity of EPR might contribute to partial serpentinization of the oceanic lithosphere. However, the EPR is a very fast spreading system and likely the serpentinization at these locations is limited or, in some places, close to zero (Kerrick, 2002). The next location prone to serpentinization is located beneath TR. We propose that sea-water infiltrated through a fault system developed during the transpression and plate reorganization period (10–15 Ma) proposed by Manea et al. (2005). A last site where water might infiltrate deep into the oceanic lithosphere is the outer rise, the place where the slab bulges as it resists the bend caused by subduction. This hypothesis seems to be confirmed by a recent study carried out offshore Nicaragua, where bending-related faulting of the incoming Cocos plate at the MAT cuts across the oceanic crust, penetrating deep into the mantle and promoting hydration of the cold crust and upper mantle (Ranero et al., 2003). Once the slab enters into subduction, the *P–T* conditions change and the slab starts to dehydrate. We show that sediments are the first to dehydrate at depths corresponding to the location of the proposed serpentinized mantle wedge, 50% of the stored water being actually released. The oceanic crust also contribute to the hydration of the mantle wedge with ~50% of the accumulated water discharged into the overlying mantle. Finally, a deep (180–200 km), strong (~90% H_2O released) and localized dehydration occurs when the serpentinized oceanic lithosphere beneath TR crosses the choke point. The petrogenesis of K-rich lavas has been subject of debate because the enrichment in potassium can be achieved by several processes like crystal fractionation, sediment subduction, crustal contamination, and melt/fluid metasomatism (Rogers et al., 1987; Luhr, 1997; Carlson and Nowell, 2001). A study by Chung et al. (2001) indicates that the slab related hydrous fluids could play an effective role in the mantle source enrichment and high potassium magmatism in the Northern Taiwan volcanic zone. In our model slab dehydration occur at depths comparable with the slab depth beneath El Chichón suggesting possible fluid related mantle metasomatism, which may play a significant role in the origin of the K-rich rocks. A recent study of Macpherson et al. (2006) shows that adakitic magmatism does not require an unusual hot (or young) subducted slab and can be generated where a substantial influx of fluids is added to the mantle. Another study of Selles et al. (2004) proposed the origin of the Quaternary Nevado de Longavi volcano (located in the Andean Southern Volcanic Zone and having high Ba/Th, Sr/Y and La/Yb ratios) to be related with the subduction of Mocha Fracture Zone, which is proposed to carry significant amounts of water stored in the serpentinized lithosphere beneath it. Whether El Chichón indeed holds an adakitik-like signature or not, need to be addressed in future detailed studies. We conclude that TR serpentine strong dehydration triggers partial melting in the mantle above the subducting slab and beneath El Chichón, explaining its unusual location and probably distinct composition within the Mexican volcanic arcs.

Acknowledgments

We thank Yuri Taran, Luca Ferrari, William Bandy and an anonymous reviewer for constructive reviews. Ivan Savov, Colin Macpherson and Daniel Selles are also acknowledged for discussion on the adakitic magmatism and slab dehydration. This project is financed by PAPIT no IN105607. Numerical simulations were performed at DGSCA-UNAM Supercomputer Center (KanBalam), Mexico.

Appendix A

Thermal modeling benchmark used to find the best fitting model for the observed gravity and magnetic anomalies (Model F). The semitransparent triangle shows the location of the serpentinized mantle wedge. White dots are the seismicity from Bravo et al., 2004.

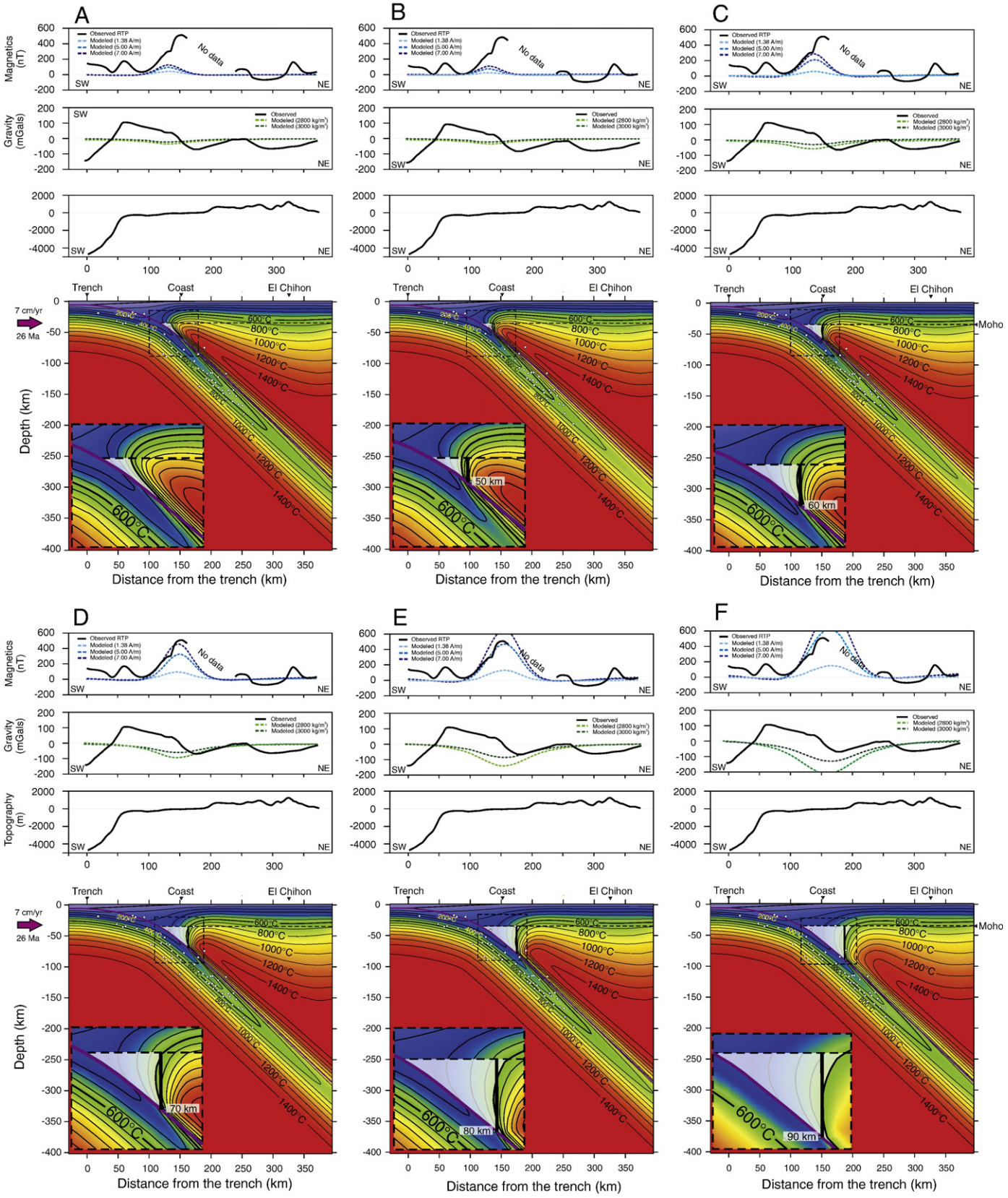

References

Arkani-Hamed, J., 1989. Thermoviscous remanent magnetization of oceanic lithosphere inferred from its thermal evolution. J. Geophys. Res. 94 (B12), 17,421–17,436.

Banerjee, S.K., 1980. Magnetism of the oceanic crust — evidence from ophiolite complexes. J. Geophys. Res. 85, 3557–3566.

Blakely, R.J., 1983. Statistical averaging of marine anomalies and the aging of the oceanic crust. J. Geophys. Res. 88, 2289–2296.

Blakely, R.J., 1995. Potential theory in gravity and magnetic applications. Cambridge University Press. 441 pp.

Blakely, R.J., Brocher, T.M., Wells, R.E., 2005. Subduction-zone magnetic anomalies and implications for hydrated forearc mantle. Geology 33 (6), 445–448. doi:10.1130/G21447.1.

Bostock, M.G., Hyndman, R.D., Rondenay, S., Peacock, S.M., 2002. An inverted continental Moho and serpentinization of the forearc mantle. Nature 417, 536–538.
Bravo, H., Rebollar, C.J., Uribe, A., Jimenez, O., 2004. Geometry and state of stress of the Wadati–Benioff zone in the Gulf of Tehuantepec, Mexico. J. Geophys. Res. 109, B04307. doi:10.1029/2003JB002854.
Carlson, R.W., Nowell, G.M., 2001. Olivine-poor sources for mantle-derived magmas: Os and Hf isotopic evidence from potassic magmas of the Colorado plateau. Geochem. Geophys. Geosyst. 2 (6). doi:10.1029/2000GC000128.
Christensen, N.I., 1966. Elasticity of ultrabasic rocks. J. Geophys. Res. 71, 5921–5931.
Chung, S.-L., Wang, K.-L., Crawford, A.J., Kamenetsky, V.S., Chen, C.-H., Lan, C.-Y., Chen, C.-H., 2001. High-Mg potassic rocks from Taiwan: implications for the genesis of orogenic potassic lavas. Lithos 59, 153–170.
Damon, P.E., Montesinos, E., 1978. Late Cenozoic volcnaism and metallogenesis over anactive Benioff zone in Chiapas, Mexico. Ariona Geolgical Soc. Digest, vol. XI, pp. 155–168.
De Ignacio, C., Cartineiras, P., Marque, A., Oyarzun, R., Lillo, J., Lopez, I., 2003. El Chichon volcano (Chiapas volcanic belt, Mexico) transitional calc-alkaline to adakitic-like magmatism: petrologic and tectonic implications. Int. Geol. Rev. 45, 1020–1028.
DeMets, C., Gordon, R., Argus, D., Stein, S., 1994. Effect of recent revisions to the geomagnetic reversal time scale on estimates of current plate motions. Geophys. Res. Lett. 21, 2191–2194.
Dunlop, D.J., Prevot, M., 1982. Magnetic properties and opaque mineralogy of drilled submarine intrusive rocks. Geophys. J.R. Astron. Soc. 69, 763–802.
Dziak, R.P., Fox, C.G., Embley, R.W., Nabelek, J.L., Braunmiller, J., Koski, R.A., 2000. Recent tectonics of the Blanco Ridge, eastern Blanco Tranform fault zone. Mar. Geophys. Res. 21 (5), 423–450.
Engdahl, E.R., Villaseñor, A., 2002. Global seismicity: 1900–1999. In: Lee, W.H.K., Kanamori, H., Jennings, P.C., Kisslinger, C. (Eds.), International Handbook of Earthquake and Engineering Seismology, Part A, chapter 41. Academic Press, pp. 665–690.
Espíndola, J.M., Macías, J.L., Tilling, R.I., Sheridan, M.F., 2000. Volcanic history of El Chichón volcano (Chiapas, Mexico) during the Holocene, and its impact on human activity. Bull. Volcanol. 62, 90–104.
Fox, P.J., Opdyke, N., 1973. Geology of the oceanic crust: magnetic properties of oceanic rocks. J. Geophys. Res. 78 (23), 5139–5154.
Garcia-Palomo, A., Macias, J.L., Espindola, J.M., 2004. Strike-slip faults and K-alkaline vocanism at El Chichon volcano southeastern Mexico. J. Volcanol. Geotherm. Res. 136, 247–268. doi:10.1016/j.jvolgeores.2004.04.001.
Hacker, B.R., Abers, G.A., Peacock, S.M., 2003. Subduction Factory 1. Theoretical mineralogy, densities, seismic wave speeds, and H_2O contents. J. Geophys. Res. 108. doi:10.1029/2001JB001127.
Hall, J.M., Fisher, B.E., Walls, C.C., Hall, S.L., Johnson, H.P., Bakor, A.R., Agrawal, V., Persaud, M., Sumaiang, A.M., 1987. Vertical distribution and alteration of dikes in a profile through the Troodos ophiolite. Nature 326, 780–782.
Harrison, C.G.A., Carle, H.M., 1981. Intermediate wavelength magnetic anomalies over ocean basins. J. Geophys. Res. 86, 11,585–11,599.
Hayling, K.L., Harrison, C.G.A., 1986. Magnetization modeling in the North and equatorial Atlantic Ocean using MAGSAT data. J. Geophys. Res. 91, 12,423–12,443.
Johnson, P.H., Atwater, T., 1977. Magnetic study of basalts from the Mid-Atlantic Ridge, lat 37°N. Geol. Soc. Amer. bull. 88, 637–647.
Kanjorsky, N.M., 2003. Cocos Plate structure along the Middle America Subduction Zone off Oaxaca and Guerrero, Mexico: Influence of subducting plate morphology on tectonics and seismicity. PhD Thesis, University of California, San Diego.
Kawamoto, T., Herving, R.L., Holloway, R., 1996. Experimental evidence for a hydrous transition zone in the Earth's early mantle. Earth Planet. Sci. Lett. 142, 587–592.
Kent, D.V., 1975. Post-depositional detrital remanent magnetism in reconstituted deep sea sediment. Proceedings Takesi Nagata Conference (June 1974, University of Pittsburgh, Pittsburgh), pp. 85–95.
Kent, D.V., Honnorez, B.M., Opdyke, N.D., Fox, P.J., 1978. Magnetic properties of dredged oceanic gabbros and the source of marine magnetic anomalies. Geophys. J. R. Astron. Soc. 55, 513–537.
Kerrick, D., 2002. Serpentine seduction. Science 298, 1344–1345.
Kesson, S., Ringwood, A.E., 1989. Slab-mantle interactions. Sheared and refertillised garnet peridotite xenoliths-samples of Wadati–Benioff zone? Chem. Geol. 78, 83–96.
Kidd, R.G.W., 1977. A model for the formation of the upper oceanic crust. Geophys. J. R. Astron. Soc. 50, 149–183.
Klitgord, K.D., Mammerickx, J., 1982. Northern east Pacific Rise; magnetic anomaly and bathymetric framework. J. Geophys. Res. 87 (138), 6725–6750.
Luhr, J.F., 1997. Extensional tectonics and the diverse primitive volcanic rocks in the western Mexican volcanic belt. Can. Mineral. 35, 473–500.
Luhr, J.F., Carmichael, I.S.E., Varekamp, J.C., 1984. The 1982 eruptions of El Chichon volcano, Chiapas, Mexico: Mineralogy and petrology of the anhydrite-bearing pumices. J. Volcanol. Geotherm. Res. 23, 29–108. doi:10.1016/0377-0273(84)90057-X.
Luyendyk, B.P., Day, R., 1982. Paleomagnetism of the Samail ophiolite, Oman. 2. The Wadi Kadir gabbro section. J. Geophys. Res. 87 (B13), 10903–10917.
Macías, J.L., Arce, J.L., Mora, J.C., Espíndola, J.M., Saucedo, R., Manetti, P., 2003. The ~550 BP Plinian eruption of el Chichón volcano, Chiapas, México: explosive volcanism linked to reheating of a magma chamber. J. Geophys. Res. 108 (ECV3), 1–18.
Macpherson, C.G., Dreher, S.T., Thirlwall, M.F., 2006. Adakites without slab melting: high pressure differentiation of island arc magma, Mindanao, the Philippines. Earth Planet. Sci. Lett. 243, 581–593.
Manea, V.C., Manea, M., 2006. The origin of modern Chiapanecan volcanic arc in southern Mexico inferred from thermal models. In: Rose, William I., Bluth, Gregg J.S., Carr, Michael J., Ewert, John W., Patino, Lina C., Vallance, James W. (Eds.), ch2: "Volcanic Hazards in Central America. GSA Special Paper, vol. 412, pp. 27–38.
Manea, M., Manea, V.C., Kostoglodov, V., 2003. Sediment fill of the Middle America Trench Inferred from the gravity anomalies. Geofis. Int. 42 (4), 603–612.
Manea, M., Manea, V.C., Ferrari, L., Kostoglodov, V., Bandy, W., 2005. Tectonic evolution of the Tehuantepec Ridge. Earth Planet. Sci. Lett. 238, 64–77.
Muller, M.R., Robinson, C.J., Minshull, T.A., White, R.S., Bickle, M.J., 1997. Thin crust beneath ocean drilling program borehole 735B at the Southwest Indian Ridge? Earth Planet. Sci. Lett. 148 (1–2), 93–107.
Nelson, S.A., Gonzalez-Caver, E., Kyser, T.K., 1995. Constraints of the origin of alkaline and calc-alkaline magmas from the Tuxtlas Volcanic Field, Veracruz, Mexico. Contrib. Mineral. Petrol. 122, 191–211.
Nixon, G.T., 1982. The relationship between Quaternary volcanism in central México and the seismicity and structure of the subducted ocean lithosphere. Geol. Soc. Amer. bull. 93, 514–523.
North American Magnetic Anomaly Group (NAMAG), 2002. Magnetic anomaly map of North America; Processing, compilation, and geologic mapping applications of the new digital magnetic anomaly database and map of North America: Denver, U.S. Department of the Interior and U.S. Geological Survey, scale 1:10,000,000, plus 31 p. booklet, http://pubs.usgs.gov/sm/mag_map/.
O 'Hanley, D.S., 1996. Serpentinites: Records of tectonic and petrological history. Oxford University Press, New York. 277 pp.
Ohtani, E., 2005. Recent progress in experimental mineral physics: phase relations of hydrous systems and the role of water in slab dynamics. Mantle: Structure, Composition, and Evolution. . Monograph Series, vol. 160. American Geophysical Union, pp. 321–334.
Omori, S., Kamiya, S., Maruyama, S., Dapeng, Z., 2002. Morphology of the intraslab seismic zone and devolatilization phase equilibria of the subducting slab peridotite. Bull. Earthq. Res. Inst. Univ. Tokyo 76, 455–478.
Ono, S., 1998. Stability limits of hydrous minerals in sediment and mid-ocean ridge basalt compositions: implications for water transport in subduction zones. J. Geophys. Res. 103 (B8), 18,253–18,267.
Pardo, M., Suarez, G., 1995. Shape of the subducted Rivera and Cocos plates in southern Mexico: seismic and tectonic implications. J. Geophys. Res. 100, 12,357–12,373.
Pariso, J.E., Johnson, P.H., 1993. Do low crustal rocks record reversals of the Earth's magnetic field? Magnetic petrology of oceanic gabbros from ocean drilling program hole 735B. J. Geophys. Res. 98 (B9), 16,013–16,032.
Parker, R.L., 1973. The rapid calculation of potential anomalies. Geophys. J. R. Astron. Soc. 31, 447–455.
Parker, R.L., Huestis, S.P., 1974. The inversion of magnetic anomalies in the presence of topography. J. Geophys. Res. 79 (11), 1587–1593.
Peacock, S.M., 2001. Are the lower planes of double seismic zones caused by serpentine dehydration in subducting oceanic mantle? Geology 29, 299–302.
Poli, S., Schmidt, M.W., 2002. Petrology of subducted slabs. Annu. Rev. Earth Planet. Sci. 30, 1–29.
Ranero, C.R., Phipps Morgan, J., McIntosh, K., Reichert, C., 2003. Bending-related daulting and mantle serpentinization at the Middle America trench. Nature 425, 367–372.
Rebollar, C.J., Espindola, V.H., Uribe, A., Mendoza, A., Vertti, A.P., 1999. Distributions of stresses and geometry of the Wadati–Benioff zone under Chiapas, México. Geofis. Int. 38 (2), 95–106.
Rogers, N.W., Hawkesworth, C.J., Mattey, D.P., Harmon, R.S., 1987. Sediment subduction and the source of potassium in orogenic leucitites. Geology 15, 451–453.
Rüpke, L.H., Morgan, J.P., Hort, M., Connolly, J.A.D., 2004. Serpentine and the subduction zone water cycle. Earth Planet. Sci. Lett. 223, 17–34.
Rye, R.O., Luhr, J.F., Wasserman, M.D., 1984. Sulfur and oxygen isotope systematics of the 1982 eruptions of El Chichon volcano. Chiapas, Mexico. J. Volcanol. Geotherm. Res. 23, 109–123.
Saad, A.F., 1969. Magnetic properties of ultramafic rocks from Red Mountain, California. Geophysics 34, 974–987. doi:10.1190/1.1440067.
Scambelluri, M., Bontazzi, P., Trommsdorff, V., Vannucci, R., Hermann, J., Gomez-Pugnaire, M.T., Lopez-Sanchez Viscaino, V., 2001. Incompatible element-rich fluids released by antigorite breakdown in deply subducted mantle. Earth Planet. Sci. Lett. 192, 457–470.
Schmidt, M.W., Poli, S., 1998. Experimental base water budgets for dehydrating slabs and consequences for arc magma generation. Earth. Planet. Sci. Lett. 163, 361–379.
Selles, D., Rodriguez, A.C., Dungan, M.A., Naranjo, J.A., Gardeweg, M., 2004. Geochemistry of Nevado de Longavi Volcano (32.2°S): a compositionally atypical arc volcano in the Southern Volcanic Zone of the Andes. Rev. Geol. Chile 31 (2), 293–315.
Syracuse, E.M., Abers, G.A., 2006. Global compilation of variations in slab depth beneath arc volcanoes and implications. G3 7 (5), Q05017. doi:10.1029/2005GC001045 ISSN 1525–2027.
Taran, Y.A., Fischer, T.B., Pokrovsky, B.G., Sano, Y., Armienta, M.A., Macias, J.L., 1998. Geochemistry of the volcano-hydrothermal system of El Chichón volcano, Chiapas, Mexico. Bull. Volcanol. 59, 436–449.
Tepley III, F.J., Davidson, J.P., Tilling, R.I., Arth, J.G., 2000. Magma mixing, recharge, and eruption histories recorded in plagioclase phenocrysts from El Chichon Volcano, Mexico. J. Petrol. 41 (9), 1397–1411.
Tivey, M.A., Johnson, P.H., Fleutelot, C., Hussenoeder, S., Lawrence, R., Waters, C., Wooding, B., 1998. Direct measurements of magnetic reversal polarity boundaries in a cross-section of oceanic crust. Geophys. Res. Lett. 25 (19), 3631–3634.
Vasicek, J.M., Frey, H.V., Thomas, H.H., 1988. Satellite magnetic anomalies and the Middle American Trench. Tectonophysics 154, 19–24.
Vine, F.J., Matthews, D.H., 1963. Magnetic anomalies over mid-ocean ridges. Nature 199, 947–949.
Wilson, D.S., 1996. Fastest known spreading on the Miocene Cocos-Pacific plate boundary. Geophys. Res. Lett. 23 (21), 3003–3006.
Ziagos, J.P., Blackwell, D.D., Mooser, F., 1985. Heat flow in southern Mexico and thermal effects of subduction. J. Geophys. Res. 90, 5410–5420.

View publication stats